Photocatalytic Water Oxidation: Tuning Light-Induced Electron Transfer by Molecular Co4O4 Cores

ARTICLE *in* JOURNAL OF THE AMERICAN CHEMICAL SOCIETY · JUNE 2012

Impact Factor: 12.11 · DOI: 10.1021/ja303951z · Source: PubMed

9 AUTHORS, INCLUDING:

Giuseppina La Ganga
Università degli Studi di Messina
13 PUBLICATIONS **346** CITATIONS
SEE PROFILE

Mirco Natali
University of Ferrara
27 PUBLICATIONS **414** CITATIONS
SEE PROFILE

Fausto Puntoriero
Università degli Studi di Messina
107 PUBLICATIONS **2,759** CITATIONS
SEE PROFILE

Sebastiano Campagna
Università degli Studi di Messina
244 PUBLICATIONS **12,387** CITATIONS
SEE PROFILE

Photocatalytic Water Oxidation: Tuning light-induced Electron Transfer by Molecular Co_4O_4 cores.

Serena Berardi,[†] Giuseppina La Ganga,[‡] Mirco Natali,[§] Irene Bazzan,[†] Fausto Puntoriero,[‡] Andrea Sartorel,[*,†,] Franco Scandola,[*,§,] Sebastiano Campagna,[‡,*] Marcella Bonchio[†,*]

[†]ITM-CNR and Department of Chemical Sciences, University of Padova, via F. Marzolo 1, 35131 Padova (Italy), [‡]Dipartimento di Chimica Inorganica, Chimica Analitica e Chimica Fisica, Università di Messina and Centro Interuniversitario per la Conversione Chimica dell'Energia Solare (sez. Messina), via Sperone 31, 98166 Messina (Italy), [§]Chemistry Department, University of Ferrara and Centro Interuniversitario per la Conversione Chimica dell'Energia Solare (sez. Ferrara), via L. Borsari 46, 44121 Ferrara (Italy).

KEYWORDS: photo-induced electron transfer, flash photolysis, cobalt cubanes, artificial photosynthesis, structure-reactivity LFER analysis

Supporting Information Placeholder

ABSTRACT: Isostructural cubane-shaped catalysts $[Co^{III}_4(\mu\text{-}O)_4(\mu\text{-}CH_3COO)_4(p\text{-}NC_5H_4X)_4]$, **1-X** (X = H, Me, *t*-Bu, OMe, Br, COOMe, CN), enable water oxidation under dark and illumination conditions, where the primary step of photo-induced electron transfer obeys to Hammett LFER behavior. Ligand design and catalyst optimization are instrumental for sustained O_2 productivity with quantum efficiency up to 80% at λ>400 nm thus opening a new perspective for in-vitro molecular photosynthesis

Aerobic life on Earth relies on a perpetual series of light-activated redox events, involving multiple and sequential photo-induced transfer of electrons and protons. Oxygenic photosynthesis is one prominent example, mastering the photo-oxidation of water, as electron and proton source, to build energy-rich carbohydrates, used as food and thus providing a vital solar fuel.[1-3] With a similar perspective, light-activated water oxidation is also the crucial step of artificial photosynthesis.[4-5] This is the off-leaf transposition of the natural machinery, finalized to the continuous production of hydrogen, as renewable and carbon-neutral energy vector. The challenge herein is a generally low quantum efficiency (QE), which is mainly dictated by the high energy cost of the water oxidation step, by far the up-hill bottleneck of the overall process. Lowering of this barrier with a bio-inspired strategy, can be accomplished by a tailored design of metal-based multi-electron catalysts.[5] These latter can foster the photo-induced removal of electrons and protons from metal-aquo intermediates via low energy pathways, eventually powered by visible light.[5]

State-of-the-art water oxidation catalysts (WOCs) are generally based on metal oxide colloids[6-11] or bulk surfaces,[12-13] and only few examples have been actually reported and proved where discrete molecular complexes can activate photocatalytic cycles.[14-19] Molecular WOCs have a formidable appeal by virtue of a tunable set of ligands affecting the redox and kinetic properties of all photo-generated intermediates and reactive transients. One promising case stems from the interplay of carboxylate and pyridine ligands that can stabilize a tetra-cobalt core, with a cubane arrangement[20] and WOC properties.[21-22] The resulting complex with formula $[Co^{III}_4(\mu\text{-}O)_4(\mu\text{-}CH_3COO)_4(NC_5H_5)_4]$ (**1-H**) deserves particular attention since: (i) cobalt is a low-cost and abundant metal, (ii) its tetra-nuclear oxo core mimics the natural Oxygen Evolving Complex of Photosystem II,[20-22] (iii) it stands as the homogeneous analog of the amorphous cobalt phosphate oxide/hydroxide film (Nocera's Co-Pi catalyst),[12] whose electrocatalytic potential has been recently exploited within light-activated devices.[23-25]

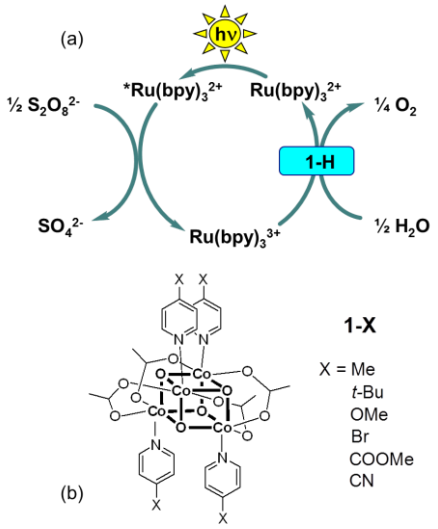

Scheme 1. (a) Light-driven water oxidation with the $Ru(bpy)_3^{2+}$ / $S_2O_8^{2-}$ system catalyzed by **1-H**. (b) Structural representation of **1-X** (X = Me, *t*-Bu, OMe, Br, COOMe, CN).

Indeed, molecular **1-H** can leverage water photooxidation cycles, by the combined presence of the photosensitizer $Ru(bpy)_3^{2+}$ (bpy = 2,2'-bipyridine) and persulfate anion, $S_2O_8^{2-}$, as the sacrificial electron acceptor (Scheme 1a, for a complete reaction scheme see SI). The resulting system, in water at pH=7, can reach a quantum efficiency of 60%

in terms of O_2 photo-conversion,[21] but the reaction kinetics and the overall productivity level off at ca. 30% of the sacrificial persulfate consumption.[21-22] The weakness herein is the irreversible decomposition of the ruthenium sensitizer, switching off the process before completion and preventing long-term operation, and/or recharge protocols.

Our study targets ligand modification and catalyst optimization to boost photoinduced electron transfer (ET), photosynthetic yields and QEs up to the outstanding value of 80%, while providing key descriptors of fundamental mechanistic aspects. Our approach focus on diverse *para*-substituted pyridines selected as terminal ligands of the cubane cluster, thus exerting a direct conjugation to each of the four cobalt sites. To this aim the isostructural series with formula $[Co^{III}_4(\mu\text{-}O)_4(\mu\text{-}CH_3COO)_4(p\text{-}NC_5H_4X)_4]$, hereafter **1-X** (X = Me, *t*-Bu, OMe, Br, COOMe, CN, Scheme 1b) has been screened for WOC under dark and illumination conditions. The impact of ligand substitution has been evaluated on (i) the electrocatalytic properties of the cobalt cubane, (ii) the rate of primary photo-induced ET events (Scheme 1a), (iii) the photosynthetic performance for O_2 production. An unprecedented structure-reactivity analysis emerges herein, highlighting the importance of ET tuning within a photosynthetic sensitizer/catalyst system by stereo-electronic ligand modification.

Table 1. Water Oxidation by **1-X** isostructural catalysts.

X[a]	η (V)[b]	k (10^8 $M^{-1}s^{-1}$)[c]	E^1_{Co4} (mV)[d]	Q.E. (%)[e]
OMe	0.57	2.51	877	80[f]
Me	0.52	1.92	880	30
t-Bu	0.50	1.39	855	10
H	0.55	1.33	926	26
Br	0.53	0.60	990	32
COOMe	0.51	0.70	1040[g]	46
CN	0.51	0.14	1081[g]	26

[a] substituent in *para*-position on the pyridine ligand, see Scheme 1b. [b] overpotential of water discharge in 0.2 M aqueous phosphate buffer (pH=7), determined at an anodic current value of 50 μA. [c] bimolecular rate constant for ET in eq. (1) in 50:50 acetonitrile : 10 mM aqueous borate buffer (pH = 8). [d] $E_{1/2}$ (**1-X**$^+$/**1-X**) in 50:50 CH_3CN/10 mM aqueous borate buffer (pH = 8). [e]quantum efficiency obtained for the photochemically-driven process (λ_{exc} = 450 nm). Note that, according to the usual photoreaction scheme (SI), the here reported QE is twice the quantum yield. [f] maximum value observed with freshly prepared solutions of **1-OMe**, see text. [g] $E_{1/2}$ in 50:50 CH_3CN/10 mM aqueous phosphate buffer (pH = 7) since the waves in 50:50 CH_3CN/10 mM aqueous borate buffer (pH = 8) are not resolved due to overlapping with water oxidation discharge, see figures S3-S4.

The isostructural complexes are obtained according to literature protocols,[20] and their solution identity and stability has been confirmed by NMR and ESI-MS (Supporting Information). Inspection of the **1-X** WOC properties has been initially addressed under dark conditions, by evaluating the water discharge overpotentials (η) with cyclic voltammetry (CV) analysis. These experiments confirm that **1-X** can actually perform water oxidation, with overpotentials varying in a narrow range (0.50-0.57 V, Table 1 and figure S2), but with no apparent ordering effect as a function of the pyridine substituent. The impact of ligand substitution has been then explored under irradiation conditions, within the sacrificial $Ru(bpy)_3^{2+}/S_2O_8^{2-}$ cycle. In this system, photocatalytic turnovers are triggered by sequential "*hole scavenging*" events, involving consecutive ET steps from the cobalt cubane to photogenerated $Ru(bpy)_3^{3+}$.[26]

The primary electron-transfer rate (equation 1), is accessible through flash photolysis technique.

$$\textbf{1-X} + Ru(bpy)_3^{3+} \rightarrow \textbf{1-X}^+ + Ru(bpy)_3^{2+} \qquad (1)$$

In these experiments a given concentration of oxidized sensitizer is generated "instantaneously" (i.e., within 10 ns) by photoreaction of the pristine $Ru(bpy)_3^{2+}$ with the $S_2O_8^{2-}$ sacrificial acceptor, and its reaction with the catalyst is monitored over a relatively wide time window (0-100 ms). These experiments show that $Ru(bpy)_3^{3+}$ (detected by the bleach at 450 nm) is reduced back to $Ru(bpy)_3^{2+}$ with kinetics dependent on the catalyst concentration as monitored by the absorbance increase at 450 nm. The bimolecular rate constant for the ET process can be then obtained, assuming pseudo-first order kinetic conditions, by linear plots of rate constants vs. catalyst concentration (Figure 1a).

For **1-H** in buffered water, primary ET was previously found to have a bimolecular rate constant, k = 1.2-1.6 10^7 $M^{-1}s^{-1}$.[21] Under those conditions, however, the recovery of $Ru(bpy)_3^{2+}$ never reached completion in the flash photolysis experiments. This was mainly ascribed to a low thermodynamic driving force dictating the ET process in buffered water, where the redox couples $Ru(bpy)_3^{3+}/Ru(bpy)_3^{2+}$ and **1-H**$^+$/**1-H** exhibits similar potentials (1.06 V and 1.05 V respectively vs Ag/AgCl, NaCl 3M).[21] The acceptor-donor redox gap can be remarkably enhanced in 50:50 CH_3CN/10 mM aqueous borate buffer (pH = 8) where the experimental potentials turn out to be 1.202 and 0.926 V, respectively (figure S3). The mixed solvent not only guarantees the proper thermodynamic boost for quantitative ET and complete recovery of the $Ru(bpy)_3^{2+}$ absorption, but brings about a strong acceleration of the ET rate with $k_H = 1.33 \cdot 10^8$ $M^{-1}s^{-1}$, that is one order of magnitude higher than in buffered water[21] (Table 1 and Figure 1). This is a key observation, as the time-domain of photo-induced ET within the photosynthetic assembly is pivotal for the required multi-hole accumulation upon sequential ET, and the sensitizer stability. This latter is a major requirement for durability of artificial systems applied to water splitting for a viable hydrogen economy (see also SI).

In the mixed solvent, complete recovery of the $Ru(bpy)_3^{2+}$ absorption is obtained with all the isostructural **1-X** complexes. Moreover a remarkable ligand effect is observed on the ET kinetics as a function of the pyridine substituent, with k_X in the range $(0.14 - 2.51) \cdot 10^8$ $M^{-1}s^{-1}$ (Table 1 and Figure 1). A linear Hammett free energy relationship (LFER) is obtained by plotting $\log(k_X/k_H)$ versus the substituent σ constants. The Hammett analysis provides a negative slope value, ρ=-1.3, indicating that photoinduced ET is favored by electron-rich pyridine ligands (Figure 1b).[27] While a similar approach has been previously re-

ported in light-activated porphyrin-dyads,[28] this evidence is unprecedented for photosynthetic assemblies involving multi-metal cores.

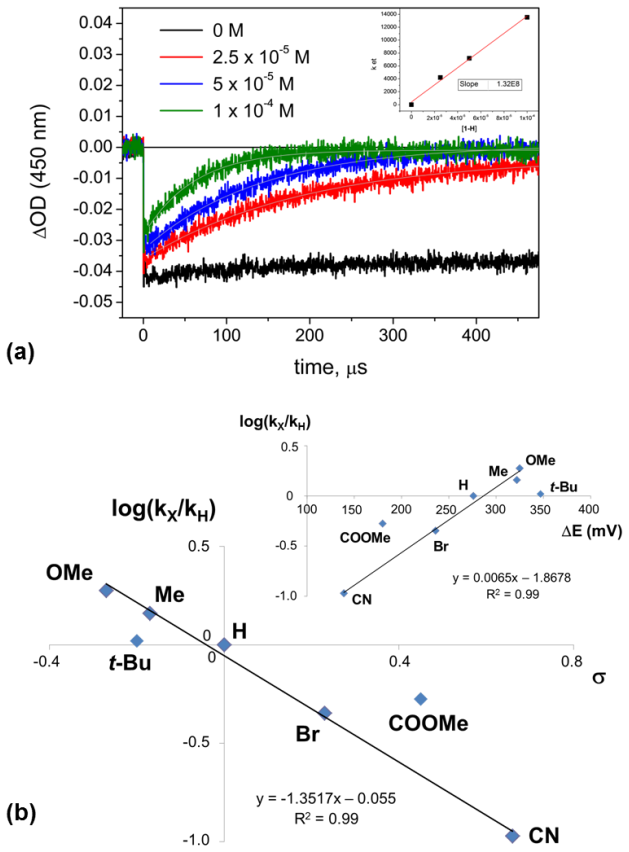

Figure 1. (a) Flash photolysis experiments (λ_{exc} = 355 nm) in 50:50 acetonitrile : 10 mM aqueous borate buffer (pH = 8) containing 5.0×10^{-5} M $Ru(bpy)_3^{2+}$ and 0-1.0×10^{-4} M **1-H**, and (inset): linear fit of kinetic rate constants vs. [**1-H**] plot for obtaining the bimolecular rate constant. (b) Hammett linear free energy relationship (LFER) plot of photoinduced ET rate constants (see text and Table 1) and (inset): plot of photoinduced ET rate constants *vs.* redox potential gap ΔE= E ($Ru(bpy)_3^{3/2+}$) – E (**1-X**$^+$/**1-X**).

The direct participation of the cobalt core[29] is also confirmed by the parallel analysis of the **1-X**$^+$/**1-X** redox potentials in CH_3CN/buffered water media (Table 1, Supporting Information, Figures S3-S4 and Figures S8-S14). Indeed, the $\log(k_X/k_H)$ values correlate with the redox potential gap ΔE= {$E_{1/2}$ ($Ru(bpy)_3^{3+/2+}$) – $E_{1/2}$ (**1-X**$^{+/0}$)}, see inset in figure 1b. This observation confirms that photoinduced ET rate increases with increasing the sensitizer/catalyst ΔE, and then it occurs in the Marcus normal region of classical electron transfer theory being accelerated by a higher thermodynamic driving force.[27]

While time-resolved spectroscopy dissects the first event of the photocatalytic cycle (eq. 1), the overall performance of the system is probed by evaluating: (i) the oxygen production yield, (ii) the catalytic turnover number (TON) and (iii) the quantum efficiency. To this aim, the oxygenic activity of the **1-X** series has been investigated in the presence of an excess of the $Ru(bpy)_3^{2+}/S_2O_8^{2-}$ couple. In a typical experiment, irradiation at λ>400 nm of **1-X** (18 μM) in 50:50 acetonitrile : 10 mM aqueous borate buffer (pH = 8) containing 1 mM $Ru(bpy)_3^{2+}$ and 5 mM $S_2O_8^{2-}$ leads to continuous oxygen production with the time-evolution profiles reported in Figure 2. Under the conditions explored, the kinetics obey to a zero order law, up to >80% of persulfate consumption, likely depending on the applied photon-flux, which maintains a stationary state of photogenerated- $Ru(bpy)_3^{3+}$.[30]

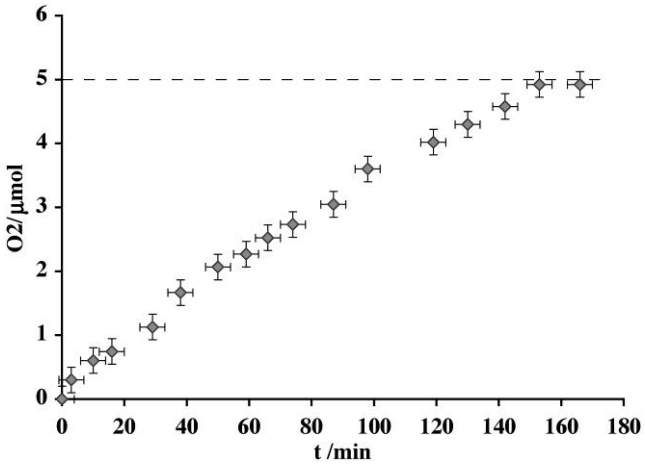

Figure 2. Oxygen production kinetics by [**1-COOMe**] = 18 μM, [$Ru(bpy)_3^{2+}$]= 1 mM, [$S_2O_8^{2-}$] = 5 mM in 50:50 acetonitrile : 10 mM borate buffer (2 ml, pH=8), λ_{irr} > 400 nm.

At variance with what observed in aqueous buffer,[21-22] in the mixed solvent, oxygen evolution occurs until quantitative consumption of the sacrificial electron acceptor (the persulfate anion $S_2O_8^{2-}$), corresponding to a total of 140 turnovers (TON= (*mol* O_2)/(*mol* cat)) per **1-H**. Such major improvement of the photosynthetic performance can result from faster hole scavenging kinetics, which leads to an improved stability of the $Ru(bpy)_3^{2+}$ photosensitizer, preventing its self-degradation under catalytic turnover.

The most relevant descriptor addressing performance in photoinduced processes, is by no doubt, the resulting quantum efficiency, that in the specific case of water oxidation, is defined as the amount of absorbed photons that are actually used to produce O_2. The QE for the **1-X** catalysts are reported in Table 1. In particular, a record value of 80% has been observed for **1-OMe**, setting a new benchmark in photoactivated water oxidation catalysis.[30]

At variance with the primary ET process, the QE trend is not showing a straightforward dependence on the ligand electronic effect. The observed QE order turns out as follows: OMe > COOMe > Me ≈ H ≈ Br≈ CN > *t*-Bu (Table 1). This result is probably related to an overall balance of competing factors crowning over the diverse steps of the oxygen release mechanism, including water coordination equilibria and possible nucleophilic attack favored by electron withdrawing substituents. The final scenario is nevertheless converging on the supremacy of the **1-OMe** term, bringing about the fastest ET and the exceptional QE of 80% determined for oxygen evolution under visible light irradiation (λ=450 nm).[31]

In summary, ligand design provides a valuable tool for shaping the multi-nuclear structure, stereoelectronic properties and ultimately the photo-assisted reactivity of molecular water oxidation catalysts. Structure-reactivity correlations spanning through-out the dissection of mechanistic events are expected to guide our quest towards innovative molecular systems with superior performances, and application in cost-effective artificial photosynthetic devices.

ASSOCIATED CONTENT

Supporting Information. Details of synthesis, characterization, electrochemical analysis, flash photolysis studies and oxygen evolution kinetics. This material is available free of charge via the Internet at http://pubs.acs.org.

AUTHOR INFORMATION

* andrea.sartorel@unipd.it; snf@unife.it;
campagna@unime.it; marcella.bonchio@unipd.it

ACKNOWLEDGMENT

We thank Valerio Doppio (University of Padova) for preliminary experiments. Financial support from MIUR (FIRB Nanosolar RBAP11C58Y), University of Padova (PRAT 2010 CPDA104105/10 and Progetto Strategico 2008 HELIOS prot. STPD08RCX) and Fondazione Cariparo (Nanomode Progetti di Eccellenza 2010) is gratefully acknowledged.

REFERENCES

(1) Gust, D.; Moore, T. A.; Moore, A. L. *Acc. Chem. Res.* **2009**, *42*, 1890.
(2) Gray, H. B. *Nat. Chem.* **2009**, *1*, 7.
(3) Lewis, N. S.; Nocera, D. G. *Proc. Natl. Acad. Sci. U. S. A.* **2006**, *103*, 15729.
(4) Meyer, T. J. *Nature* **2008**, *451*, 778.
(5) Sartorel, A.; Carraro, M.; Toma, F.M.; Prato, M.; Bonchio, M. *En. Env. Sci.* **2012**, *5*, 5592.
(6) Youngblood, W. J.; Lee, S.-H. A.; Kobayashi, Y.; Hernandez Pagan, E. A.; Hoertz, P. G.; Moore, T. A.; Moore, A. L.; Gustand, D.; Mallouk, T. E. *J. Am. Chem. Soc.* **2009**, *131*, 926.
(7) La Ganga, G.; Nastasi, F.; Campagna, S.; Puntoriero, F. *Dalton Trans.* **2009**, 9997.
(8) Zhang, J.; Grzelczak, M.; Hou, Y.; Maeda, K.; Domen, K.; Fu, X.; Antonietti, M.; Wang, X. *Chem. Sci.* **2012**, *3*, 443.
(9) Najafpour, M.M.; Ehrenberg, T.; Wiechen, M.; Kurz P. *Angew. Chem., Int. Ed.* **2010**, *49*, 2233.
(10) Jiao, F.; Frei, H. *Energy Environ. Sci.* **2010**, *3*, 1018.
(11) Hocking, R. K.; Brimblecombe, R.; Chang, L.-Y.; Singh, A.; Cheah, M. H.; Glover, C.; Casey, W. H.; Spiccia, L. *Nat. Chem.* **2011**, *3*, 461.
(12) Kanan, M. W.; Nocera, D. G. *Science* **2008**, *321*, 1072.
(13) Gerken, J. B.; McAlpin, J. G.; Chen, J. Y. C.; Rigsby, M. L.; Casey, W. H.; Britt, R. D.; Stahl, S. S. *J. Am. Chem. Soc.* **2011**, *133,* 14431.
(14) Herrero, C.; Quaranta, A.; Leibl, W.; Rutherford, A. W.; Aukauloo, A. *En. Env. Sci.* **2011**, *4*, 2353.
(15) Duan, L.; Tong, L.; Xu, Y.; Sun, L. *En. Env. Sci.* **2011**, *4*, 3296.
(16) Huang, Z.; Luo, Z.; Geletii, Y. V. Vickers, J. W.; Yin, Q.; Wu, D.; Hou, Y.; Ding, Y.; Song, J.; Musaev, D. G.; Hill, C. L.; Lian, T. *J. Am. Chem. Soc.* **2011**, *133*, 2068.
(17) Puntoriero, F.; La Ganga, G.; Sartorel, A.; Carraro, M.; Scorrano, G.; Bonchio, M.; Campagna, S. *Chem. Commun.* **2010**, *46*, 4725.
(18) Karlsson, E. A.; Lee, B. L. Åkemark, T.; Johnston, E. V.; Karkas, M. D.; Sun, J. L.; Hansson, O.; Backvall, J. E.; Åkemark, B. *Angew. Chem., Int. Ed.* **2011**, *50*, 11715.
(19) Concepcion, J. J.; Jurss, J. W.; Brennaman, M. K.; Hoertz, P. G.; Patrocinio, A. O. T.; Murakami Iha, N. Y.; Templeton, J. L.; Meyer, T. J. *Acc. Chem. Res.* **2009**, *42*, 1954.
(20) Chakrabarty, R.; Bora, S. J.; Das, B. K. *Inorg. Chem.* **2007**, *46*, 9450.
(21) La Ganga, G.; Puntoriero, F.; Campagna, S.; Bazzan, I.; Berardi, S.; Bonchio, M.; Sartorel, A.; Natali, M.; Scandola, F. *Faraday Discuss.* **2012**, *155*, 177.
(22) McCool, N. S.; Robinson, D. M.; Sheats, J. E.; Dismukes, G. C. *J. Am. Chem. Soc.* **2011**, *133*, 11446.
(23) Steinmiller, E. M. P.; Choi, K.-S. *Proc. Natl. Acad. Sci. U.S.A.* **2009**, *106*, 20633.
(24) Zhong, D. K.; Gamelin, D. R. *J. Am. Chem. Soc.* **2010**, *132*, 4202.
(25) Reece, S. Y.; Hamel, J. A.; Sung, K.; Jarvi, T. D.; Esswein, A. J.; Pijpers, J. J. H.; Nocera, D. G. *Science* **2011**, *334*, 645.
(26) Puntoriero, F.; Sartorel, A.; Orlandi, M.; La Ganga, G.; Serroni, S.; Bonchio, M.; Scandola, F.; Campagna, S. *Coord. Chem. Rev.*, **2011**, *255*, 2594.
(27) Photoinduced ET rates appear to be mainly controlled by the thermodynamic driving force, as a well-behaved linear Hammett correlation is obtained with the experimental redox potentials of **1-X** (Supporting Information, Figure S5). However other stereo-electronic factors come into play, likely determined by the details of the sensitizer/catalyst supramolecular interaction. While the negative deviation of **1-*t*-Bu** in the LFER plot of Figure 1 can easily be assigned to steric hindrance, the positive deviation of **1-COOMe** compensating for the thermodynamic fall is under investigation.
(28) Gust, D.; Moore, T.A.; Moore, A.L.; Kang, H.K.; DeGraziano, J.M.; Liddell, P.A., Seely, G.R. *J. Phys. Chem.* **1993**, *97*, 13637.
(29) McAlpin, J. G.; Stich, T. A.; Ohlin, C. A.; Surendranath, Y.; Nocera, D. G.; Casey, W. H.; Britt, R. D. *J. Am. Chem. Soc.* **2011**, *133*, 15444.
(30) Turnover frequencies (TOF) are frequently used to compare the efficiency of photo-driven catalytic processes. However TOF values are proportional to quantum yields, with proportionality linked to various parameters, including photon flux. A wide range of apparent TOF values can be obtained for the same process, upon variation of the photon flux. For such reasons, any comparison between TOF of photo-driven processes obtained in different experimental conditions is misleading. Comparison between photo-driven TOF with those pertaining to dark processes, and vice-versa, although appealing, should also be avoided. The only relevant parameter, as mentioned above, is the quantum efficiency, QE. For the sake of comparison, TOF values presented in Table 1 (1.3-7.1·10^{-5} s^{-1}) are determined with a photon flux of 2·10^{-9} einstein s^{-1}, at λ=450 nm.
(31) While **1-OMe** remains stable in the timescale of the photocatalytic experiments, its prolonged ageing in the reaction mixture leads to a modification of the Uv-Vis spectrum (Supporting Information, Figure S6) and a parallel reduction of the quantum efficiency up to 30% upon pre-incubation of the catalyst for 24h. Inspection of the ^{1}H-NMR spectrum shows a minor line broadening, possibly consistent with a partial leaching of paramagnetic Co(II) ions in solution (Supporting Information, Figure S7), eventually responsible for the observed drop of the catalytic activity.

Photocatalytic Water Oxidation: Tuning light-induced Electron Transfer by Molecular Co_4O_4 cores.

Serena Berardi, Giuseppina La Ganga, Mirco Natali, Irene Bazzan, Fausto Puntoriero, Andrea Sartorel, Franco Scandola, Sebastiano Campagna and Marcella Bonchio